Molecular noise of capping protein binding induces macroscopic instability in filopodial dynamics

Pavel I. Zhuravlev and Garegin A. Papoian[1]

Department of Chemistry, University of North Carolina, Chapel Hill, NC 27599-3290

Edited by Peter G. Wolynes, University of California at San Diego, La Jolla, CA, and approved April 30, 2009 (received for review December 15, 2008)

Capping proteins are among the most important regulatory proteins involved in controlling complicated stochastic dynamics of filopodia, which are dynamic finger-like protrusions used by eukaryotic motile cells to probe their environment and help guide cell motility. They attach to the barbed end of a filament and prevent polymerization, leading to effective filament retraction due to retrograde flow. When we simulated filopodial growth in the presence of capping proteins, qualitatively different dynamics emerged, compared with actin-only system. We discovered that molecular noise due to capping protein binding and unbinding leads to macroscopic filopodial length fluctuations, compared with minuscule fluctuations in the actin-only system. Thus, our work shows that molecular noise of signaling proteins may induce micrometer-scale growth–retraction cycles in filopodia. When capped, some filaments eventually retract all the way down to the filopodial base and disappear. This process endows filopodium with a finite lifetime. Additionally, the filopodia transiently grow several times longer than in actin-only system, since less actin transport is required because of bundle thinning. We have also developed an accurate mean-field model that provides qualitative explanations of our numerical simulation results. Our results are broadly consistent with experiments, in terms of predicting filopodial growth retraction cycles and the average filopodial lifetimes.

amplification | stochastic chemical kinetics | growth–retraction cycles | stochastic switch | mechano-chemical sensing

Eukaryotic motile cells project finger-like protrusions, called filopodia, to probe their environment and help guide cell motility (1). They play important roles in neuronal growth (2), wound healing (3), and cancer metastasis (4). The filopodial structure consists of parallel actin filaments, cross-linked into bundles by actin-binding proteins, all of which is enclosed by the cell's plasma membrane (1, 5). Despite their importance in eukaryotic biology and human health, the physical mechanisms behind filopodial regulation and dynamics are poorly understood, including what drives ubiquitous growth–retraction cycles and eventual filopodial disappearance (1–7). Using stochastic simulations of filopodial dynamics, we have discovered that molecular noise due to binding/unbinding of a capping protein results in macroscopic growth–retraction fluctuations, compared with minuscule fluctuations in the actin-only system. Because of rare fluctuations some filaments eventually retract all the way down to the filopodial base and disappear. In contrast to prior computational models that predicted stable filopodia at steady state, our simulations show that filopodial lifetimes are finite. We have also developed an accurate mean-field model that provides insights into filament disappearance kinetics.

A comprehensive computational model of a filopodium should contain the following features: mechanical interactions including membrane dynamics, protrusion force, and retrograde flow; chemical interactions, including actin polymerization and depolymerization; and biological signaling interactions that control the filopodia dynamics turnover. The first mean-field model for filopodial growth addressed the interplay between filament growth and diffusional actin transport (8). A subsequent work highlighted the importance of the interactions between the membrane and filament barbed ends (9). Our own previous study treated both polymerization and diffusion in a fully stochastic fashion (10). In that model, the filopodia grow to some steady-state length, and subsequently exhibit only slight fluctuations (10). Thus, no essential dynamics occurs after the steady state is reached, a finding similar to those of other prior filopodial simulations (8, 9), implying an essentially infinite filopodial lifetime and no turnover.

Although it is not well known whether the turnover is driven externally or internally, it is plausible that internal biochemical reaction network dynamics is a significant contributor. For instance, capping proteins bind to the barbed ends of actin filaments preventing polymerization (11). Their efforts are countered by formins (12), anticapping processive motors that attach to the barbed ends and may effectively increase polymerization rate up to fivefold (12). In this work, we investigated the influence of two regulating proteins on the filopodial turnover process. The mechanochemical model that we use here to describe the filopodial dynamics is fully stochastic, using the Gillespie algorithm to calculate simulation steps (Fig. 1). It consists of the following processes: (*i*) the diffusion of proteins from the cytosol at the filopodial base to the tip; (*ii*) the force applied by the membrane on individual filaments; (*iii*) the actin filament polymerization and depolymerization at the barbed end; (*iv*) the depolymerization at the pointed end and the induced retrograde flow v_{retr} of the filopodium as a whole; (*v*) capping of the filaments that stops polymerization (11); (*vi*) binding of formin to the barbed end that increases effective polymerization rate fivefold (12). The filopodium is split into compartments with diffusion realized as stochastic hops between them. Membrane force is taken into account by effectively decreasing the polymerization rates (see *Materials and Methods* and ref. 10 for more details). The parameters, such as reaction rates and concentrations, are given in Table 1.

The addition of capping proteins and formins results in very different, more complex growth dynamics (Fig. 2), in contrast to the actin-only model in ref. 10, where the observed length of the filopodium was stationary. In particular, filopodial length fluctuations become *macroscopic*, increasing from $<$100 nm in a model without these proteins to a few micrometers, on the order of the length of filopodia. In addition, a clearly identifiable retraction phase appears, with a lifetime of $\sim$100 s. The mechanism is this: when an individual filament is capped, the retrograde flow makes it retract—the filament will eventually disappear if uncapping does not occur quickly enough. If the filament number becomes less than a minimum needed to overcome the membrane force, the filopodium collapses.

These large-amplitude oscillations of filopodial length observed in our simulations are the consequence of the amplification of molecular noise of capping protein. This amplification is possible because of the timescale separation between fast polymerization and retrograde flow processes and slow off-rates of formin and capping protein. Because the regulatory proteins are present in

Author contributions: P.I.Z. and G.A.P. designed research, performed research, analyzed data, and wrote the paper.

The authors declare no conflict of interest.

This article is a PNAS Direct Submission.

[1]To whom correspondence should be addressed. E-mail: gpapoian@unc.edu.

www.pnas.org/cgi/doi/10.1073/pnas.0812746106

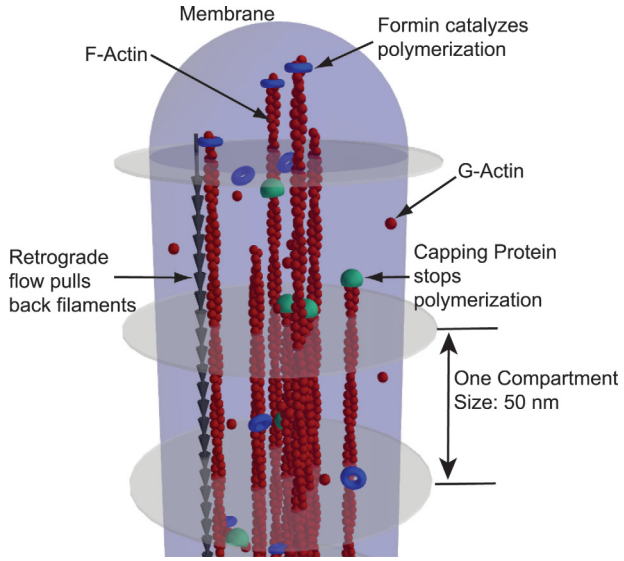

Fig. 1. Schematic representation of the mechanochemical model used in this work. Simulation details are elaborated in the text.

very low concentrations (<100 nM), their noise is highly discrete (13–21), randomly driving back-and-forth transitions from fast growth to fast retraction for each filament. Such a highly fluctuating behavior should be advantageous from the point of view of efficiency of a filopodium as an environmental sensor, in analogy to near-critical systems, where large fluctuations are indicative of large corresponding susceptibilities. Indeed, we found that the filopodial length is significantly more sensitive to the change in membrane force in a system with capping proteins and formins than in a system with just actin.

To compare our predictions with prior and future experiments, we computed filopodial lifetime distribution from 2,048 Gillespie trajectories (Fig. 2 *Lower*). Experimentally reported lifetimes are on the order of several minutes, consistent with our results (6, 22–26). We found that computed filopodial lifetimes strongly depend on the amplitude of the individual filament length fluctuations (Fig. 3).

Table 1. Model variables and parameters

Mechanics	
Half-actin monomer size	$\delta = 2.7$ nm
Number of filaments	$N = 16$
Membrane force	$f = 10$ pN
Diffusion rate	$k_D = 5\,\mu\text{m}^2\,\text{s}^{-1}(2{,}000\,\text{s}^{-1})$*
Membrane fluctuation	$\sigma_d = 20$ nm
Retrograde flow speed	$v_{\text{retr}} = 70$ nm/s
(De)Polymerization rates	
Free barbed end	$k_A^+ = 11.6\,\mu\text{M}^{-1}\,\text{s}^{-1}(21.8\,\text{s}^{-1})$
Formin-anticapped	$k_{FA}^+ = 53.2\,\mu\text{M}^{-1}\,\text{s}^{-1}(100\,\text{s}^{-1})$
Depolymerization	$k_A^- = 1.4\,\text{s}^{-1}$
(Anti)Capping rates	
Formin on-rate	$k_F^+ = 10\,\mu\text{M}^{-1}\,\text{s}^{-1}(18.8\,\text{s}^{-1})$
Formin off-rate	$k_F^- = 0.0667\,\text{s}^{-1}$
Capping rate	$k_C^+ = 3.5\,\mu\text{M}^{-1}\,\text{s}^{-1}(6.6\,\text{s}^{-1})$
Uncapping rate	$k_C^- = 0.04\,\text{s}^{-1}$
Bulk concentrations	
Actin	$C_A = 10\,\mu$M
Capping protein	$C_C = 50$ nM
Formin	$C_F = 40$ nM; 80 nM

*Reaction and diffusion rates in parentheses in "seconds" units depend on the compartment volume. In our computations the compartment volume was fixed, with compartment length of $l_D = 50$ nm and a filopodial diameter of 150 nm.

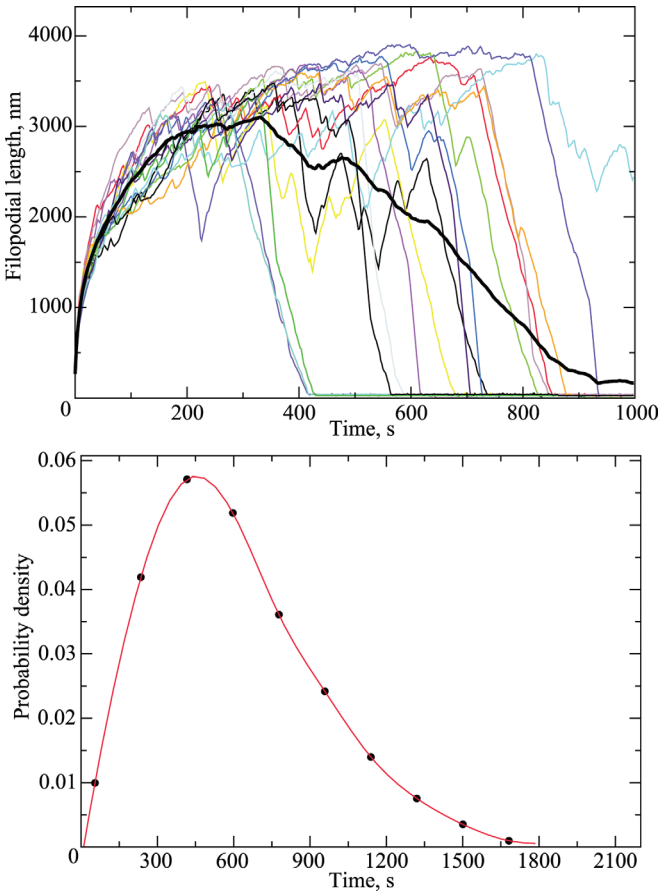

Fig. 2. Microscopic oscillations endow a filopodium with a finite lifetime. (*Upper*) Sixteen individual trajectories are shown from stochastic simulations of filopodial growth and retraction with 80 nM formin and 50 nM capping protein. The average over trajectories is indicated with a thick black line. Individual trajectories undergo turnover—growth–retraction oscillations on a micrometer scale—which is induced by molecular noise of regulatory proteins. (*Lower*) Distribution of the filopodial lifetime calculated from 2,048 trajectories at 40 nM formin and 50 nM capping protein.

To gain further insight into the observed noise amplification phenomenon, we investigated how the capping protein and formin concentrations influence the magnitude of the filopodial macroscopic fluctuations. To measure them, we created a stationary state by allowing the tips of disappearing filaments to stay at the filopodial base and eventually uncap. As one might have anticipated, the fluctuation amplitude grows with increasing capping protein concentration. However, formin quenches these oscillations such that the fluctuation amplitude depends mainly on the ratio of the capping protein to formin concentrations (Fig. 3 *Upper*). Overall, filopodial lifetime strongly depends on the amplitude of the individual filament length fluctuations (Fig. 3 *Lower*).

To shed light into the kinetics of filopodial retraction, we address the question of how such long timescale processes (hundreds of seconds) emerge from the much faster constituent kinetic rates (filament uncapping rate, $k_C^- = (25\,\text{s})^{-1}$ is the slowest rate in our model). We elaborate below on a simple mean-field model to estimate the rate for filament disappearance. We consider a filament in the bundle of N anticapped filaments of stationary length, L, computed in our prior work (10) (see Table 1 for the definition of variables):

$$L = \frac{k_D l_D}{N}\left(\frac{C_A\delta}{v_{\text{retr}}} - \left(1 + \frac{k_A^-\delta}{v_{\text{retr}}}\right)\frac{1}{k_{FA}^+}e^{f\delta/Nk_BT}\right). \quad [1]$$

We keep track of a single filament as various binding/unbinding events occur. After formin unbinds (with off-rate, k_F^-), the filament

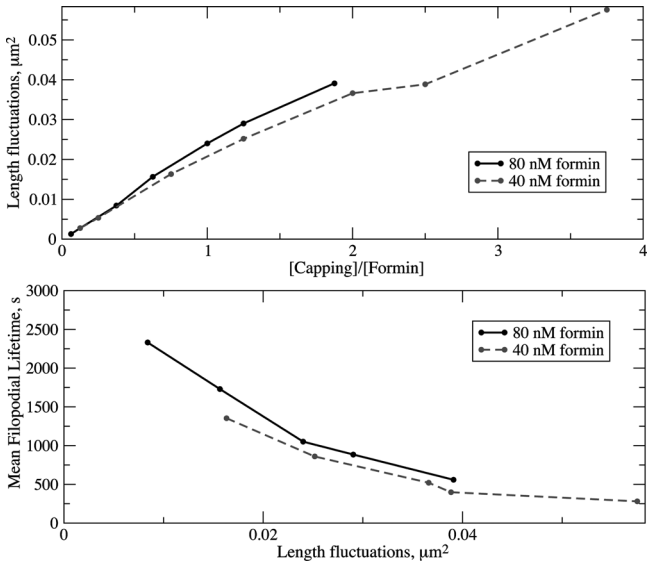

Fig. 3. The amplitude of filament length fluctuations depends on the concentrations of regulating proteins, mainly, on their ratio. These fluctuations, in turn, largely determine the mean filopodial lifetime.

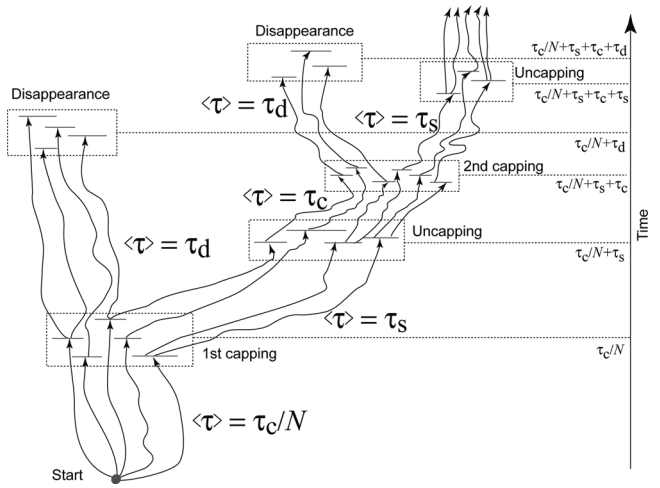

Fig. 4. The system dynamics is executed on a multidimensional lattice on which a stochastic propagator enacts a random walk. Eventually, a trajectory arrives to a sublattice where one filament is capped. Mean-field average time for that is $\bar{\tau}_c/N$. From there some trajectories lead to filament disappearance due to retrograde flow and some to filament uncapping with respective statistical weights of p and $1-p$ and mean-field average times τ_d and $\bar{\tau}_s$. After uncapping, all trajectories will pass through the phase area where this filament is capped again after mean-field average time $\bar{\tau}_c$. Then again, it may either disappear after time τ_d or uncap after time $\bar{\tau}_s$ with weights p and $1-p$.

may either become capped and start retracting or rebind formin, with the latter being more likely. The ratio of probabilities for capping and anticapping is proportional to the ratio of the on-rates for capping protein and formin, $C_C k_C^+$ and $C_F k_F^+$, where C_C and C_F are capping protein and formin concentrations, respectively. The regulatory proteins are not consumed during polymerization (unlike actin), thus, we can assume bulk concentrations at the tip. Overall, the average capping time for a filament may be estimated as $\bar{\tau}_c = (k_F^-)^{-1}(C_C k_C^+)^{-1}(C_F k_F^+)$.

The computational model for filopodial dynamics is essentially a multidimensional lattice on which a stochastic propagator enacts a random walk. If the filament is capped, it may either fully retract and disappear or become uncapped and grow back. Thus, many possible trajectories on the lattice must be considered. Each distinct trajectory is characterized by a certain probability of occurrence and the overall time for filament disappearance. The trajectories may be grouped according to how may times the filament has been capped and uncapped before it disappears. In the following analytical estimation, we calculate average time of disappearance in each group of paths described above by using a mean-field approximation, instead of carrying out a full path integral calculation (Fig. 4). Such a group of paths may be thought of as a particular event scenario. We then average the rates from each group with statistical weights of the scenarios; the weights are computed exactly.

In a bundle of N filaments the average time to wait for a capping event is $\bar{\tau}_c/N$. Once a filament is capped, it starts to retract under retrograde flow. It may either fully shrink and disappear or uncap and regrow (first trajectory bifurcation; see Fig. 4). If uncapping does not occur, it takes $\tau_d \approx L/v_{\text{retr}}$ for the filament to fully shrink and disappear. The probability to follow this scenario is therefore $p = \exp(-k_C^- \tau_d)$. The alternative scenario—the filament uncapping and resuming growth after average time $\bar{\tau}_s$ of shrinking—occurs with $1-p$ probability. To find the typical shrinking time (the time it takes for a capped filament to uncap), $\bar{\tau}_s$, one has to average over the exponential distribution for uncapping up to τ_d (since for longer times the filament has fully retracted according to the first scenario),

$$\bar{\tau}_s = \int_0^{\tau_d} \tau P(\tau) d\tau = \frac{1}{k_C^-}\left[1 - e^{-k_C^- \tau_d}\left(1 + k_C^- \tau_d\right)\right]. \qquad [2]$$

After uncapping, the filament starts to regrow until the next capping. If x is the position of the barbed end with respect to filopodial base, then the regrowth speed is $v_g(x) = \dot{x} = C_A(1 - x/L)k_{FA}^+\delta - v_{\text{retr}}$, where the steady-state G-actin concentration gradient has been taken into account (C_A is the bulk concentration at the filopodial base). We solve this equation to obtain the filament length after regrowing for time $\bar{\tau}_c$, the average time until the next capping event:

$$x(\bar{\tau}_c) = \tilde{L} - \left[\tilde{L} - x(0)\right]\exp\left(-C_A k_{FA}^+ \delta \bar{\tau}_c / L\right), \qquad [3]$$

where $\tilde{L} = L\left(1 - \frac{v_{\text{retr}}}{C_A k_{FA}^+ \delta}\right)$. With a very large polymerization rate provided by formin, the exponential factor is essentially zero, so the new length is $x(\bar{\tau}_c) \approx \tilde{L} \approx L$, as $v_{\text{retr}} \ll C_A k_{FA}^+ \delta$. Therefore, if a capped filament is uncapped, it quickly catches up with the others at steady-state length. Thus, a filament either retracts after average time $\bar{\tau}_c/N + \tau_d$ with probability p, or returns to initial state after time $\bar{\tau}_c/N + \bar{\tau}_s$ with probability $1-p$. This filament will be capped again after average time $\bar{\tau}_c$, and there will be second trajectory bifurcation: it will either retract with probability $(1-p)p$ at time $\bar{\tau}_c/N + \bar{\tau}_s + \bar{\tau}_c$, or start growing again with probability $(1-p)^2$ at time $\bar{\tau}_c/N + \bar{\tau}_s + \bar{\tau}_c + \bar{\tau}_s$. Each subsequent trajectory bifurcation leads to a longer time (lower rate) for filament disappearance, but also is less likely to occur. To get the full rate one has to average the disappearance rates over all scenarios:

$$\lambda = \sum_{n=0}^{\infty} \frac{p_n}{\tau_n} = \sum_{n=0}^{\infty} \frac{p(1-p)^n}{a + bn} = \frac{p}{a}\,{}_2F_1\left(1, \frac{a}{b}; \frac{a}{b} + 1; 1 - p\right), \qquad [4]$$

where ${}_2F_1$ is the hypergeometric function; $a = \bar{\tau}_c/N + \tau_d$; $b = \bar{\tau}_c + \bar{\tau}_s$.

Thus, the average time for filament disappearance is $\bar{\tau} = 1/\lambda$, where λ is given in Eq. **4**. We ran simulations with different numbers of filaments at two formin concentrations, looking for an average time of disappearance of one filament. Because there are multiple filaments in these simulations, and several of them may be capped at the same time, we need to take into account a possibility that the first capped filament is not the first to disappear,

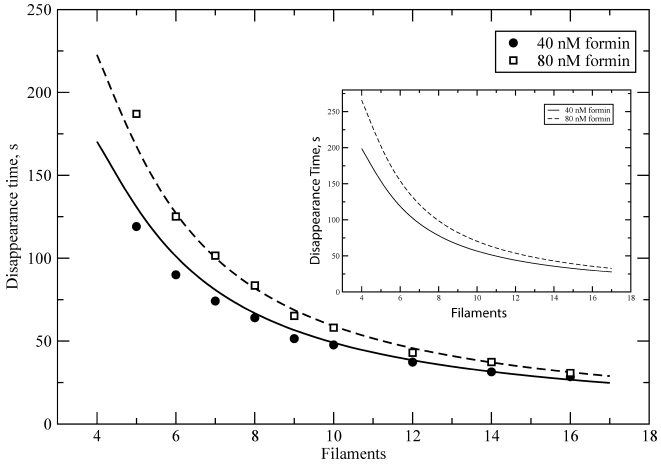

Fig. 5. Rate of individual filament disappearance from a bundle of N filaments at $C_C = 50$ nM and $C_F = 40$ nM (circles, solid lines) and 80 nM (squares, dashed lines). The symbols show simulation results. Solid and dashed lines are computed by combining the disappearance for a single filament, given by Eq. **4**, with the scenarios of other filaments disappearing, which had capped later. We used the following expression to estimate the average time for any of the bundle filaments to fully retract, $\tau_{\text{multi}} = (1-p)^{n_c-1}\lambda^{-1} + (1-(1-p)^{n_c-1})(\bar{\tau}_c n_c/N + \tau_d)$, where, $n_c = \lambda^{-1}/(\bar{\tau}_c/N)$, indicates the average number of simultaneously capped filaments, and the remaining symbols are defined in text. In this expression, the first term corresponds to the first capped filament disappearing first, whereas the second term accounts for the possibility of one of the other $n_c - 1$ capped filaments following the scenario of quickly disappearing without uncapping even once. (*Inset*) Bare disappearance times for single filaments, λ^{-1}, computed from Eq. **4**, where the effect of other filament retractions is not taken into account.

to directly compare the results from simulations with the analytical estimates. This possibility might occur if the first capped filament uncaps and grows back, while another capped filament quickly retracts. In Fig. 5, the average filament disappearance time is computed by considering not only $\bar{\tau} = 1/\lambda$, but also taking into account the contributions from the simultaneous retraction of other filaments. The comparison between simulations and analytical results, where the latter did not contain adjustable parameters, showed good agreement (see Fig. 5).

Another interesting result that we observed was that the longest filopodia grow to ≈4.5 times the size of those simulated without formins and capping proteins [in our prior work (10)]. The explanation for this follows: a key factor limiting the filopodial length is insufficient actin transport (8, 10). A mean-field estimation for the stationary length (Eq. **1**) follows from equating the actin flux from the established gradient and actin consumption by N polymerizing barbed ends (10). Because the latter is proportional to N, a smaller number of filaments require less actin for growth; therefore, a thinner filopodium can grow longer before the diffusive G-actin transport again becomes a limiting factor. As filaments cap and disappear, N decreases, hence, the increase in the length. When too few filaments remain to oppose the force of the membrane load, the bundle withdraws, resulting in the eventual filopodial disappearance. One can speculate another interesting consequence of bundle thinning: it may induce mechanical buckling instability, due to diminution of the mechanical rigidity of the F-actin bundle. In light of the recent suggestion that filopodia with >10 filaments are mechanically stable (27), our current finding of filament bundle thinning may turn out to be an important mechanism for mechanical collapse of filopodia due to buckling.

In summary, we have shown in this work that capping proteins exert a dramatic effect on filopodial dynamics. Introducing them allowed us to create a computational model that predicts a finite lifetime of filopodia. The resulting filopodial length dynamics has a remarkable feature: discrete noise of regulatory proteins that are in very low concentration becomes greatly amplified. Because of timescale separation, this slow discrete noise triggers the fast retrograde flow and polymerization processes resulting in oscillations of filopodial length macroscopic in space and time. This result suggests that experimentally observed filopodial growth–retraction turnover dynamics (5–7) may be partially driven by the internal noise of the filopodial mechanochemical network. Large-amplitude fluctuations in filopodia may be important with respect to their sensory role. In particular, a molecular system having oscillations of this magnitude is expected to be easily perturbed by small external forces, either mechanical or chemical in origin, in analogy with large susceptibilities seen in near-critical systems with large fluctuations. The noise amplification described in this work, arising from discrete noise in a low copy number of some of the reaction network species, is related to stochastic switching in biochemical signal transduction, for example, when a cell needs to make a binary decision (28). A similar dynamic instability is observed in microtubular growth, although in filopodia the oscillations are switched by the binding noise, and in microtubular catastrophes and rescues it is enzymatic in origin (29). In addition, by promoting filament disappearance, capping proteins thin the filopodium, reducing its mechanical rigidity. We speculate that this may be an important mechanism for creating buckling instabilities. We also investigated in detail the filament retraction kinetics, and developed a mean-field analytical estimation for the rate of disappearance of individual filaments that matches the simulation data surprisingly well. We explained the extremely slow timescale of filament disappearance, compared with bare kinetic rates, by common occurrence of multiple capping, shrinking, and regrowing events, before the filament fully retracts as a result of a rare fluctuation.

Materials and Methods

In our stochastic model of filopodial growth (10), represented in Fig. 1, we assume that the reaction processes are confined to a spatial region having a linear dimension of ζ [so-called Kuramoto length (30)], such that particles diffuse across the region quickly compared with the typical reaction times. This allows us to discretize space into compartments and model protein diffusion along the filopodium as a random walk on a one-dimensional lattice, with molecules hopping between these compartments at rates calculated from diffusion coefficients. At relevant concentrations, ζ is on the order of 100 nm at the tip of the filopodium. We chose a somewhat more conservative compartment size of $l_D = 50$ nm (10). At the filopodial base the protein concentrations are kept at their constant bulk values. Biochemical reactions within each compartment are simulated by using the Gillespie algorithm (10, 31). Polymerization rates at the tip are decreased by the membrane force via the Brownian ratchet model (8, 10). The experimentally reported uncapping frequency is about once every 30 min, however, it may be greatly increased through the actions of uncapping proteins, such as PIP2 (11). The variables and parameters for the model are given in Table 1. Further simulation details are elaborated below.

The Stochastic Model of Filopodial Growth. A mature filopodium is a bundle of a few dozen actin filaments enclosed by the cell membrane with a protein complex at the tip (32). The filopodial base is usually located within a three-dimensional actin mesh below, which forms the basis for the lamellipodium (32). In addition, bundling proteins cross-link the filaments in the bundle, but this was not included in our current model.

Typical growth and retraction speeds are within 0.1–0.2 μm/s, with filopodial lengths reaching 1–2 μm (33). In special cases, the filopodial length may reach nearly 100 μm (34). Since short filopodia are mostly straight, for simplicity we assume growth of straight filaments. Longer filopodia might tilt and bend. The possibilities of bending of the filaments and buckling of a filopodium should be addressed in future work.

Depending on the number of actin filaments, the filopodial diameter typically varies between $d = 100$ nm and 300 nm. In our simulations we used $d = 150$ nm, a number that was derived from minimizing the membrane free energy (9) and is reasonable if the number of filaments is not too large.

Our physicochemical model of filopodial growth consists of the following processes: (*i*) diffusion of proteins along the filopodial tube, providing passive transport from cell body to the filopodial tip; (*ii*) mechanical interactions between the membrane and individual filaments; (*iii*) actin filament polymerization and depolymerization processes at the barbed end; (*iv*) depolymerization at the pointed end and the induced retrograde flow v_{retr} of the bundle as a whole; (*v*) capping of the filaments that stops polymerization (11); and (*vi*) binding of formin to the barbed end which increases the effective polymerization rate fivefold (12).

Polymerization, Depolymerization. Actin filaments (F-actin) are asymmetric, with one end called "the barbed end" and the other end called "the pointed end." Because of ATP binding and subsequent hydrolysis, chemical affinities for monomers (G-actin) are different at the two ends, such that the polymerization rate at the barbed end is much higher. This leads to the motion of the filament as a whole in the direction of the barbed end (whereas individual monomer units migrate from the barbed end to the pointed end). This process is called "treadmilling" and is the biochemical basis for the cytoskeletal dynamics (35, 36), including filopodial protrusion. An actin filament consists of two protofilaments, wound up in a right-handed helix, with a pitch distance of 37 nm. Diameter of one globular actin monomer is 5.4 nm. In our simulations we increase the filament length by $\delta = 2.7$ nm on one polymerization event, since there are two protofilaments, and two monomers are needed to increase length by 5.4 nm.

The resulting double-helical filament is mechanically robust, with a persistent length, $L_p \sim 10\,\mu$m. The buckling length, or the critical length at which one filament would buckle if subject to a force F, is

$$L_b \approx \frac{\pi}{2}\sqrt{\frac{k_B T L_p}{F}}, \qquad [5]$$

where k_B is the Boltzmann constant and $k_B T = 4.1$ pN nm at room temperature (8). The equation gives $L_b \approx 100$ nm for a force $F = 10$ pN for a single filament. For weakly cross-linked bundles of N actin filaments, the buckling length of the bundle is $\sqrt{N}L_b$, whereas it is $NL_b/\sqrt{2}$ for tightly linked bundles (8). A recent work suggested that the membrane enclosure significantly increases these estimates (27).

In our model, cytosolic molecules such as G-actin, formin, or capping protein, which are in the same compartment as the filopodial tip, can attach to one of the filament ends with a probability, given by the rates k_A^+, k_{FA}^+, or k_C^+. These monomers at filament ends can also stochastically dissociate with the corresponding rates k_A^-, k_{FA}^-, or k_C^-. In prior experiments, it was shown that the actin polymerization rate rather strongly depends on the membrane force (37). Theoretical explanations were also provided (8, 38, 39). For instance, the Brownian ratchet model considers membrane fluctuations at the tip of the filopodium (38, 40). That the membrane fluctuations are sufficient to allow a G-actin monomer to fit sterically atop the filament allows a polymerization with the rate k_A^+. Thus, the effective polymerization rate $k_{A,n}$ on the nth filament equals the "bare" rate $k_{A,0}$ times the probability of the gap opening at the tip of the nth filament. A convenient relation between the loading force f_n and the polymerization rate was derived earlier (40),

$$k_n^+ = k^+ \exp\left(-\frac{f_n \delta}{k_B T}\right). \qquad [6]$$

According to Eq. **6** the on-rates for G-actin monomer addition (k_A^+ for free barbed end; k_{FA}^+ for the barbed end anticapped by formin) and capping protein (k_C^+) are modified after each timestep. The on-rate for formin, k_F^+, was assumed to be independent of the membrane fluctuations due to diminished steric constraints (12). All of the off-rates do not depend on the membrane position.

For these effective on-rates, we needed to estimate the membrane force on each individual filament, which is discussed next.

Membrane Force. According to prior studies fluctuations of a membrane sheet below micrometer scale relax on the microsecond to millisecond timescale (41–44). Chemical reactions occur on a much slower timescale (10^{-2}–10^{1} s), thus, due to this timescale separation, the membrane fluctuations may be assumed to be equilibrated at the time of each given chemical event. Each filament experiences an individual membrane force, f_n, that depends on the proximity of the filament tip to the average location of the membrane. Thus, the total membrane force f is distributed among the individual filaments, $f = \sum_n f_n$.

To calculate f_n, we assume that on average the force on a filament is proportional to the membrane-filament contact dwelling probability, which is the probability that the membrane touches that filament. That, in turn, depends on the amplitude of the membrane fluctuation near the filament and the filament length. Longer filaments are more likely to be in contact with the membrane, and feel a stronger membrane force. If the membrane fluctuations are assumed to be described by a Gaussian distribution around the membrane average position, the dwelling probability p_n for the nth filament to be in contact with the membrane is proportional to the probability that the membrane height is found below the filament end

$$p_n \sim \int_{h-h_n}^{\infty} \exp\left(-z^2/\sigma_d^2\right) dz, \qquad [7]$$

where σ_d is the average membrane fluctuation amplitude (discussed next). Once p_n is obtained, the force f_n on each filament may be computed,

$$f_n = \frac{p_n}{p} f, \qquad [8]$$

where $p = \sum_n p_n$ is a normalization factor. Then we use Eq. **6** to modify the polymerization rates.

Retrograde Flow. The filopodial dynamics are strongly controlled by the polymerization at its tip (45, 46). As was mentioned earlier, the "treadmilling" contributes to a steady backward motion of the whole actin filament bundle, called the retrograde flow. In some cells, it is believed that specific myosin motors participate in creating the retrograde flow (47). All of this is subject to the regulation by the signaling proteins, but in our current computations, we neglect these subtleties of the retrograde flow process, and assume a constant average retrograde flow speed, v_{retr}. The retrograde flow speed v_{retr} is $\approx$20–200 nm/s (46, 48–51) and we take $v_{\text{retr}} = 70$ nm/s as the default value in our simulations.

Numerical Scheme. Our computations are based on the Gillespie algorithm (31). In particular, at each simulation step two independent random numbers are chosen, where the first one determines the time of the next event $t + \delta t$ (t is the time of last event) based on the reaction rates present in the system, and the second one determines which event occurs, based on the magnitude of individual event rates. The event is chosen among the following possibilities: (*i*) G-actin monomer, capping protein or formin hopping between filopodial compartments, (*ii*) individual filament polymerization or capping events, (*iii*) depolymerization or uncapping events, and (*iv*) binding or unbinding of formin. Then, we update current time, adding δt, the numbers of proteins in compartments, filament length, and which protein is on its end according to the event that happened. We then incorporate retrograde flow and update the length of filaments again. Finally, the membrane load is partitioned among the filaments, as described above, which results in recomputing individual filament polymerization rates, according to the Brownian ratchet model.

ACKNOWLEDGMENTS. This work was supported by National Science Foundation Grant CHE-715225. All calculations were carried out using the UNC Topsail supercomputer.

1. Faix J, Rottner K (2006) The making of filopodia. *Curr Opin Cell Biol* 18:18–25.
2. Dent EW, Gertler FB (2003) Cytoskeletal dynamics and transport in growth cone motility and axon guidance. *Neuron* 40:209–227.
3. Noselli S (2002) Drosophila, actin and videotape—New insights in wound healing. *Nat Cell Biol* 4:E251–E253.
4. Lorenz M, Yamaguchi H, Wang Y, Singer RH, Condeelis J (2004) Imaging sites of n-wasp activity in lamellipodia and invadopodia of carcinoma cells. *Curr Biol* 14: 697–703.
5. Wood W, Martin P (2002) Structures in focus—Filopodia. *Int J Biochem Cell Biol* 34:726–730.
6. Miller J, Fraser SE, McClay D (1995) Dynamics of thin filopodia during sea urchin gastrulation. *Development* 121:2501–2511.
7. Chang S, Camilli PD (2001) Glutamate regulates actin-based motility in axonal filopodia. *Nat Neurosci* 4:787–793.
8. Mogilner A, Rubinstein B (2005) The physics of filopodial protrusion. *Biophys J* 89:782–795.
9. Atilgan E, Wirtz D, Sun SX (2006) Membrane and dynamics of actin-driven thin membrane protrusions. *Biophys J* 90:65.
10. Lan Y, Papoian GA (2008) The stochastic dynamics of filopodial growth. *Biophys J* 94:3839–3852.
11. Schafer DA, Jennings PB, Cooper JA (1996) Dynamics of capping protein and actin assembly in vitro: uncapping barbed ends by polyphosphoinositides. *J Cell Biol* 135:169–179.
12. Vavylonis D, Kovar DR, O'Shaughnessy B, Pollard TD (2006) Model of formin-associated actin filament elongation. *Mol Cell* 21:455–466.
13. Kepler TB, Elston TC (2001) Stochasticity in transcriptional regulation: Origins, consequences, and mathematical representations. *Biophys J* 81:3116–3136.
14. Sasai M, Wolynes PG (2003) Stochastic gene expression as a many-body problem. *Proc Natl Acad Sci USA* 100:2374–2379.
15. Korobkova E, Emonet T, Vilar JMG, Shimizu TS, Cluzel P (2004) From molecular noise to behavioural variability in a single bacterium. *Nature* 428:574.
16. Walczak AM, Onuchic JN, Wolynes PG (2005) Absolute rate theories of epigenetic stability. *Proc Natl Acad Sci USA* 102:18926–18931.
17. Weinberger LS, Burnett JC, Toettcher JE, Arkin AP, Schaffer DV (2005) Stochastic gene expression in a lentiviral positive-feedback loop: Hiv-1 tat fluctuation drive phenotypic diversity. *Cell* 122:169–182.
18. Thattai M, van Oudenaarden A (2004) Stochastic gene expressions in fluctuatiing environments. *Genetics* 167:523–530.
19. Lan Y, Wolynes P, Papoian GA (2006) A variational approach to the stochastic aspects of cellular signal transduction. *J Chem Phys* 125:124106.
20. Lan Y, Papoian GA (2006) The interplay between discrete noise and nonlinear chemical kinetics in a signal amplification cascade. *J Chem Phys* 125:154901.
21. Lan Y, Papoian G (2007) Stochastic resonant signaling in enzyme cascades. *Phys Rev Lett* 98:228301.
22. Gomez TM, Robles E, Poo M, Spitzer NC (2001) Filopodial calcium transients promote substrate-dependent growth cone turning. *Science* 291:1983–1987.
23. Jontes JD, Buchanan J, Smith SJ (2000) Growth cone and dendrite dynamics in zebrafish embryos: Early events in synaptogenesis imaged in vivo. *Nat Neurosci* 3:231–237.
24. McCroskery S, Chaudhry A, Lin L, Daniels MP (2006) Transmembrane agrin regulates filopodia in rat hippocampal neurons in culture. *Mol Cell Neurosci* 33: 15–28.
25. Portera-Cailliau C, Pan DT, Yuste R (2003) Activity-regulated dynamic behavior of early dendritic protrusions: evidence for different types of dendritic filopodia. *J Neurosci* 23:7129–7142.
26. Varnum-Finney B, Reichardt LF (1994) Vinculin-deficient pc12 cell lines extend unstable lamellipodia and filopodia and have a reduced rate of neurite outgrowth. *J Cell Biol* 127:1071–1084.

27. Pronk S, Geissler PL, Fletcher DA (2008) Limits of filopodium stability. *Phys Rev Lett* 100:258102.
28. Artyomov MN, Das J, Kardar M, Chakraborty AK (2007) Purely stochastic binary decisions in cell signaling models without underlying deterministic bistabilities. *Proc Natl Acad Sci USA* 104:18958–18963.
29. Zong C, Lu T, Shen T, Wolynes PG (2006) Nonequilibrium self-assembly of linear fibers: microscopic treatment of growth, decay, catastrophe and rescue. *Phys Biol* 3:83–92.
30. Kuramoto, Y (1984) *Chemical Oscillations, Waves and Turbulence* (Springer, Berlin).
31. Gillespie DT (1977) Exact stochastic simulation of coupled chemical reactions. *J Phys Chem* 81:2340–2361.
32. Svitkina TM, et al. (2003) Mechanism of filopodia initiation by reorganization of a dendritic network. *J Cell Biol* 160:409–421.
33. Argiro V, Bunge B, Johnson MI (1985) A quantitative study of growth cone filopodial extension. *J Neurosci Res* 13:149–162.
34. Gustafson T, Wolpert L (1961) Studies on the cellular basis of morphogenesis in the sea urchin embryo: directed movements of primary mesenchyme cells in normal and vegetalized larvae. *Exp Cell Res* 24:64–79.
35. Pantaloni D, Clainche CL, Carlier M-F (2001) Mechanism of actin-based motility. *Science* 292:1502.
36. Pollard TD, Borisy GG (2003) Cellular motility driven by assembly and dissembly of actin filaments. *Cell* 112:453–465.
37. Carlsson AE (2001) Growth of branched actin networks against obstacles. *Biophys J* 81:1907–1923.
38. Mogilner A (2006) On the edge: Modeling protrusion. *Curr Opin Cell Biol* 18:32–39.
39. Mogilner A, Oster G (2003) Force generation by actin polymerization. ii. The elastic ratchet and tethered filaments. *Biophys J* 84:1591–1605.
40. Peskin CS, Odell GM, Oster GF (1993) Cellular motions and thermal fluctuations: The brownian ratchet. *Biophys J* 65:316–324.
41. Lin LC-L, Brown FLH (2004) Brownian dynamics in fourier space: Membrane simulations over long length and time scales. *Phys Rev Lett* 93:256001.
42. Pécréaux J, Döbereiner H-G, Prost J, Joanny J-F, Bassereau P (2004) Refined contour analysis of giant unilamellar vesicles. *Eur Phys J E Soft Matter* 13:277–290.
43. Gov NS, Safran SA (2005) Red blood cell membrane fluctuations and shape controlled by atp-induced cytoskeletal defects. *Biophys J* 88:1859–1874.
44. Safran S, Gov N, Nicolas A, Schwarz U, Tlusty T (2005) Physics of cell elasticity, shape and adhesion. *Physica A* 352:171–201.
45. Mejillano MR, et al. (2004) Lamellipodial versus filopodial mode of the actin nanomachinery: pivotal role of the filament barbed end. *Cell* 118:363–373.
46. Mallavarapu A, Mitchison T (1999) Regulated actin cytoskeleton assembly at filopodium tips controls their extension and retraction. *J Cell Biol* 146:1097.
47. Heid PJ, Geiger J, Wessels D, Voss E, Soll DR (2005) Computer-assisted analysis of filopod formation and the role of myosin II heavy chain phosphorylation in dictyostelium. *J Cell Sci* 118:2225–2237.
48. Lidke DS, Lidke KA, Rieger B, Jovin TM, Arndt-Jovin DJ (2005) Reaching out for signals: Filopodia sense EGF and respond by directed retrograde transport of activated receptors. *J Cell Biol* 170:619–626.
49. Forscher P, Smith SJ (1988) Actions of cytochalasins on the organization of actin filaments and microtubules in a neuronal growth cone. *J Cell Biol* 107:1505.
50. Brown ME, Bridgman PC (2002) Retrograde flow rate is increased in growth cones from myosin IIB knockout mice. *J Cell Sci* 116:1087.
51. Huckaba TM, Lipkin T, Pon LA (2006) Roles of type II myosin and a tropomyosin isoform in regrograde actin flow in budding yeast. *J Cell Biol* 175:957.